Transport properties of an asymmetric mixture in the dense plasma regime

Christopher Ticknor, Joel D. Kress, Lee A. Collins, Jean Clérouin, Philippe Arnault, and Alain Decoster

Phys. Rev. E **93**, 063208 — Published 23 June 2016

DOI: 10.1103/PhysRevE.93.063208

Transport properties of an asymmetric mixture in the dense plasma regime

Christopher Ticknor, Joel D. Kress, and Lee A. Collins
Theoretical Division, Los Alamos National Laboratory, Los Alamos, New Mexico 87545, USA

Jean Clérouin, Philippe Arnault, and Alain Decoster
CEA, DAM, DIF, 91297 Arpajon, France
(Dated: June 8, 2016)

We study how concentration changes ionic transport properties along isobars-isotherms for a mixture of hydrogen and silver, representative of turbulent layers relevant to inertial confinement fusion (ICF) and astrophysics. Hydrogen will typically be fully ionized while silver will be only partially ionized but can have a large effective charge. This will lead to very different physical conditions for the H and Ag. Large first principles orbital free molecular dynamics (OFMD) simulations are performed and the resulting transport properties are analyzed. Comparisons are made with transport theory in the kinetic regime and in the coupled regime. The addition of a small amount of heavy element in a light material has a dramatic effect on viscosity and diffusion of the mixture. This effect is explained through kinetic theory as a manifestation of a crossover between classical diffusion and Lorentz diffusion.

PACS numbers:

I. INTRODUCTION

Mixtures display rich behavior, and this is particularly true for warm dense matter (WDM) and dense plasma systems where ionization plays a significant role in determining the properties. When there are many types of ions, then the ionization properties will vary between constituents, leading to very different coulomb couplings between species. This will influence the properties of a system and these influences will be particularly acute for strongly asymmetric mixtures. Mixture properties play a significant role in inertial confinement fusion (ICF). For example, mixing of the plastic ablator into the fuel has been used to partially explain lower than expected yields in experiments [1–4]. Understanding this behavior is crucial, so much so that experiments are designed to monitor and control mixing of the ablator into the fuel. Further motivation comes from the mixing of a gas/metal interface [5–7]. In such cases, interfaces lead to strong concentration gradients and mixing. Many astrophysical situations also involve ionic transport in mixtures for the investigation of the composition of giant planets [8] and of the sedimentation of heavy elements in white dwarf stars [9], for instance.

Efforts to understand mixtures have typically taken on one of three approaches: (i) mixing rules; (ii) simulations with model systems, such as the one component plasma (OCP) or Yukawa; or (iii) direct simulations of mixtures. (i) Mixing rules have proven successful for equation of state by systematic comparisons with simulations [10–12]. They have also been shown to be reasonable for transport coefficients for LiH [11] and CH [13] mixtures, but less has been done for more asymmetric mixtures. (ii) Models used to estimate transport properties are through the OCP model and its extension to binary ionic mixtures (BIM) and Yukawa model. The OCP and BIM are models where ions move in a uniform background of electrons. The Yukawa model includes screening effects of the electrons. A shortcoming of these methods is that decisions have to be made about the degree of ionization and screening to include in any given simulations. Typical approaches seek to produce an effective single component result for the transport properties, some via the OCP and Yukawa models [14–18]. Large Yukawa molecular dynamics (MD) studies have explored the behavior of diffusion and viscosity for a fixed ion density while the concentration is varied by simply swapping out ion types [19, 20]. This work found significant changes in both the diffusion and viscosity as concentration was changed. Other recent work is based on quantum average atom models that account for correlations of ions via a hyper-netted chain approximation [21, 22]; then by using pseudo-atom molecular dynamics [23], the entire equation of state can be obtained. (iii) The last approach is to perform direct simulations from first principles. This involves a variety of methods, all of which solve the electronic structure, examples include quantum molecular dynamics [24], path integral Monte Carlo (PIMC) [25, 26], and orbital free molecular dynamics (OFMD) [27]. Here we will focus on the use of OFMD, which has proven accurate for extracting equations-of-state and mass transport properties for the WDM regime and up to the dense plasma regime [28–32].

We study H-Ag as a prototypical light-heavy mixture. H will be fully ionized while Ag will be only partially ionized but can have a large effective charge. This will lead to very different physical conditions for the H and Ag. We will perform simulations along isobars-isotherms and look at the impact of varying concentration at several different temperatures, and we systematically study the evolution of the ionic transport properties. We imagine an interface at pressure and temperature equilibrium [33, 34] and sample different concentrations between pure H and Ag. The density varies from pure Ag at 20 g/cc to

pure H. The density of the H depends on the temperature (0.8-3.8 g/cc). We pick several temperatures between 20-2000 eV.

In the remaining paper we will first review OFMD methods and transport properties. After describing the pseudo ion in jellium (PIJ) model we will give some scaling laws for pure species. At last we discuss the results of OFMD and compare them to the PIJ model and extract some scaling laws in temperature.

II. FORMULATION

A. OFMD simulations

We have performed large OFMD simulations of H-Ag mixtures. We use the Born-Oppenheimer approximation that separates the electronic and ionic degrees of freedom so for a given ion configuration, the electronic structure is computed at equilibrium. Then classical equations of motion for the ions are numerically integrated within the isokinetic ensemble [35]. The simulation has a total number N of ions in a volume V ($n = N/V$). N is the sum of all species $N = \sum_\gamma N_\gamma$, where for the γ^{th} species, there are N_γ ions with nuclear charge Z_γ and atomic weight A_γ. Concentrations in number will be denoted by $x_\gamma = N_\gamma/N$ and we will also use for simplicity $x = N_2/N$ for the heavy element concentration. Additionally there are $N_e = \sum_\gamma N_\gamma Z_\gamma$ electrons in the volume.

The electronic density is found with a finite-temperature orbital-free density functional theory [27] treatment (TFD, Thomas-Fermi-Dirac) with the kinetic-entropic form of Perrot [36]. The electron-ion interaction is obtained from a regularization prescription [27] and the exchange-correlation from a local density Perdew-Zunger form [37]. Extensive studies were taken to optimize both the time step and FFT grid required to converge all properties. The FFT grids range between 128^3 and 256^3. Despite the statistical description of electronic density compared with an orbital description, the OFMD method has proven to be accurate for ionic transport properties for temperatures beyond 20eV [29].

For the OFMD simulations, the total pressure of the system is

$$P = nk_BT + P_{\rm conf}(V,T). \tag{1}$$

This is the sum of the ideal gas pressure of the ions (at a constant T enforced by the isokinetic thermostat) and the configurational pressure $P_{\rm conf}$, computed via the forces on ions along trajectories and averaged after the system has equilibrated.

To target a given pressure with OFMD simulations, we start with 20 g/cm^3 of pure Ag at a given temperature and match various other concentrations to the pressure of pure Ag. The concentrations studied are 0, 3, 5, 10, 25, 50, 75, and 100% silver by number. The temperatures studied are 20, 50, 100, 200, 400, 600, 1000, and 2000 eV. The mixture density ranges between 0.84 to 20 g/cm^3 at temperatures of 20 to 2000 eV. The ion number ranged from 64 for pure species simulations up to 300 for mixture simulations. The 3% Ag by number simulation had the fewest number of Ag ions at 9.

We extract the transport properties from the mixture OFMD simulations [38, 39]. The self-diffusion coefficient of a particular ion species, D_γ is computed from the integral of the velocity autocorrelation function (VACF), which is:

$$D_\gamma = \frac{1}{3}\int_0^\infty \langle \vec{v}_i(t)\cdot\vec{v}_i(0)\rangle dt, \tag{2}$$

where $\vec{v}_i$ is the velocity of the i^{th} particle (γ species), and the bracket indicates an ensemble average.

Mutual diffusion is found within the Maxwell-Stefan formulation through the integral of a correlation function:

$$D_{12} = \frac{1}{3Nx_1x_2}\int_0^\infty \langle A(t)A(0)\rangle dt \tag{3}$$
$$A(t) = x_2\sum_i^{N_1}\vec{v}_i(t) - x_1\sum_i^{N_2}\vec{v}_i(t).$$

The Darken relation,

$$D_{12} = x_1D_2 + x_2D_1, \tag{4}$$

is an approximation found by neglecting cross correlations between different species. The Darken approximation allows for quick estimate of the mutual diffusion.

The shear viscosity was computed from the autocorrelation function of the stress tensor

$$\eta = \frac{V}{k_BT}\int_0^\infty \langle P_{12}(t')P_{12}(0)\rangle dt'. \tag{5}$$

Here the bracket indicates an ensemble average, for further details see [11, 38].

We use empirical fits to the autocorrelation functions (ACF) to shorten the duration of the trajectory required to converge the transport properties [30, 40]. For our set of thermodynamic conditions the ACFs are generally not structured, and a simple exponential fit suffices to extract the desired properties. The statistical error inherent in computing correlation functions from molecular dynamics is estimated [41] as $\sqrt{2\tau/N_tdt}$ where N_tdt is the length of the trajectory and τ is the correlation time of the ACF. We usually fit the ACF over a time interval of 0 to 4τ. The length of the simulation is much longer than τ. For the viscosity, the error computed is 10% or less for all simulations. The error for the self-diffusion is less than 5%, due to the additional factor of $1/\sqrt{N_\gamma}$ from averaging the VACF over all of the ions of type γ. The convergence was tested even for high temperature simulations that contain H.

The correlation time scales of the viscosity and the mutual diffusion are typically long compared to self-diffusion time scales. This is not always the case for

hydrogen, when at several hundred eVs, the time scales become comparable. To converge all properties required a large number of time steps. The simulations required a large amount of computational resources and were run on Cielo, a Cray XE6 with AMD Opterons at Los Alamos. Typical simulations ran on 2048 cores for 24-72 hours to produce a few hundred thousand to several millions time steps.

B. Pseudo Ion in Jellium model

In the asymmetric mixture considered here, the light element (hydrogen) is in the kinetic regime because the coupling parameter $\Gamma = Q^2e^2/ak_BT$ is much smaller than 1, where Q is the ionic charge, $a = (3/4\pi n)^{1/3}$ is the Wigner-Seitz radius, and k_B is Boltzmann's constant. On the contrary the heavy element is strongly coupled due to its high ionization, see Fig. 1 (a) below. It is thus important to have a theory able to treat on a equal footing both regimes. In the weakly coupled regime, the interaction between particles α and β is described by collision frequencies given by the kinetic theory in the Fokker-Plank-Landau framework (FPL). For a Maxwellian distribution

$$\nu_{\alpha\beta} = \frac{n_\beta}{m_\alpha}\ \frac{4\sqrt{2\pi\ m_{\alpha\beta}}\ Q_\alpha^2 Q_\beta^2\ e^4\ \ln\Lambda_{\alpha\beta}}{3\ \left(k_BT\right)^{3/2}}, \tag{6}$$

where Q_α, n_α and m_α are respectively the charge, the density and the mass of specie α, and $\ln\Lambda_{\alpha\beta}$ the Coulomb logarithm for $\alpha\beta$ interactions. $m_{\alpha\beta} = m_\alpha m_\beta/(m_\alpha+m_\beta)$ is the reduced mass and e the elementary charge. For a binary mixture, the collision frequency between fully ionized light elements 1 (hydrogen) is

$$\nu_{11} = \frac{n_1}{m_1}\ \frac{4\sqrt{2\pi\ m_{11}}\ e^4\ \ln\Lambda_{11}}{3\ \left(k_BT\right)^{3/2}}, \tag{7}$$

and for interactions between light (1) and heavy (2) ionized Q times

$$\nu_{12} = \frac{n_2}{m_1}\ \frac{4\sqrt{2\pi\ m_{12}}\ Q^2\ e^4\ \ln\Lambda_{12}}{3\ \left(k_BT\right)^{3/2}}. \tag{8}$$

Using these standard collision frequencies, and defining a total collision frequency $\tilde{\nu_1} = \nu_{11} + \nu_{12}$ and $\tilde{\nu_2} = \nu_{22} + \nu_{21}$ for each species. The total collision term in a kinetic equation is the sum of binary collision terms. This suggests to define a total collision frequency ν_α for species α as the sum of the Maxwellian estimates of the collision frequencies $\nu_{\alpha\beta}$. Taking it as a reference makes the remaining coefficient (called relaxation correction) to be of order unity in all cases. The viscosity $\eta^{\rm FPL}$, the mutual diffusion $D_{12}^{\rm FPL}$ and the self-diffusions $D_\alpha^{\rm FPL}$ read [42–44]

$$\eta^{\rm FPL} = K_1\ \frac{n_1\ k_BT}{\tilde{\nu_1}} + K_2\ \frac{n_2\ k_BT}{\tilde{\nu_2}}, \tag{9a}$$

$$D_{12}^{\rm FPL} = R_{12}\ c_2\ \frac{k_BT}{\nu_{12}}\ \frac{\overline{m}}{m_1m_2}, \tag{9b}$$

$$D_\alpha^{\rm FPL} = R_\alpha\ \frac{1}{\tilde{\nu_\alpha}}\ \frac{k_BT}{m_\alpha}, \alpha = 1, 2 \tag{9c}$$

where c_2 is the heavy element mass concentration, $\bar{m} = x_1m_1 + x_2m_2$ and K_1, K_2, R_1, R_2 and R_{12} are correction factors with respect to the Maxwellian estimate of the collision frequencies, Eq. (6). These factors are called relaxation corrections since they have been evaluated by solving the linearized kinetic equations to obtain the corrections to the Maxwellian distributions associated with small gradients of concentration, velocity, and temperature. For pure element plasmas, the relaxation corrections are known [43] : $R_1 = 1.19$ and $K_1 = 0.965$, with $x_2 = 0$.

For binary mixtures, the relaxation corrections have been determined for high mass asymmetry, $m_1 \ll m_2$ [43]. In this case, K_1 is parametrized by a function of ν_{12}/ν_{11}, varying from 1 to 2 (see Appendix), whereas $K_2 = 0.965$. The relaxation correction R_{12} of the mutual diffusion is also a parametrized function of ν_{12}/ν_{11}, varying from 1 to 3.5 (see Appendix). The only quantities, which are not well-defined to our knowledge, are R_1 and R_2 assumed to be of the order of a few units. We propose in the Appendix an approximation of R_1 and R_2 assuming that they do not depend on concentration. By making the simplification of a constant Coulomb logarithm it is easy to show that the total collision frequency of the light element is strongly influenced by a small amount of the heavy element. Let x equal the proportion in number of the heavy element and Q, its ionization, the sum of the collision frequencies is proportional to inverse of $f(x) = ((1-x) + \sqrt{2}xQ^2)^{-1}$. The self diffusion will thus experience a rapid decay, proportional to $f(x)$, with a small amount of heavy element as shown in Fig. 1 (b). This effect is not observed for silver which is well outside the kinetic regime ($\Gamma \simeq 15$; see Fig. 1(a) in which the coupling parameters of hydrogen and silver are given). In Fig. 1(a) inset, we show the ionization of Ag as a function of the temperature. This shows that the ionization is near 7 at 20 eV. Then the ionization with nearly a $\sqrt{T}$ behavior increases. At 2000 eV, the ionization levels out slightly.

In the pseudo ion in jellium, the Coulomb coupling adds excess contributions to the kinetic formulas.

$$\eta = \eta^{\rm FPL} + \eta_{\rm ex}, \tag{10a}$$

$$D = D^{\rm FPL} + D_{\rm ex}, \tag{10b}$$

with a bounded Coulomb logarithm to avoid divergencies

$$\ln\Lambda \longrightarrow \max\left(\ln\Lambda\,, L_0\right) \quad \text{with} \quad L_0 = 2. \tag{10c}$$

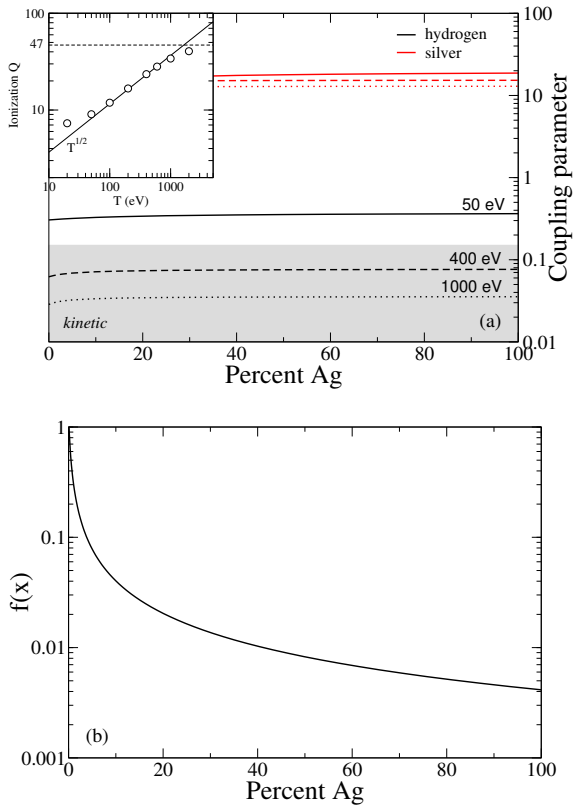

FIG. 1: (Color online) a) Coupling parameter, Γ, for hydrogen (black) and silver (red) versus concentration for 50 eV (solid line), 400 eV (dashed line) and 1000 eV (dotted line). The gray area defines the weak coupling region where kinetic formulation is the main contribution. Inset: The ionization of Ag (open circles) is shown as a function of temperature with a line showing $T^{1/2}$ scaling law. b) Plot of the function $f(x) = ((1-x)+\sqrt{2}xQ^2)^{-1}$ proportional to the inverse of the collision frequency of hydrogen mixed with silver (Q=15). x is the Ag concentration by number.

The excess contribution to viscosity is computed using the mixing rule from Ref. [14], where an effective OCP is defined, with a coupling parameter $\Gamma_{\rm eff}$ equal to

$$\Gamma_{\rm eff} = \sum_\alpha x_\alpha \, \Gamma_\alpha = \frac{\overline{Z_*^{5/3}} \; \overline{Z_*}^{1/3} e^2}{a \; k_B T}. \qquad (11)$$

Γ_α are obtained in the BIM formulation with ionizations given by More's fit, see Ref.[17, 45] for details. A smooth interpolation across coupling regimes is obtained by subtracting the corresponding kinetic viscosity of the effective pure element at $\Gamma_{\rm eff}$, Eq. (9a), from Bastea's OCP fit [15]:

$$\eta^*_{OCP} = 0.482 \; \Gamma^{-2} + 0.629 \; \Gamma^{-0.878} + 1.88 \; 10^{-3} \; \Gamma. \quad (12a)$$

Star superscript indicates dimensionless quantities. The OCP Viscosity and diffusion are functions of the coupling parameter Γ, and they are expressed in natural plasma units: $\eta/\eta_0 = \eta^*(\Gamma)$, $D/D_0 = D^*(\Gamma)$, with $\eta_0 = nM\omega_p a^2$ and $D_0 = \omega_p \; a^2$, where ω_p is the plasma frequency $\omega_p^2 = 4\pi n Q^2 e^2/M$ of species of charge Q and mass M.

The excess contribution to the mutual diffusion is computed using Darken relation, Eq. (4), with effective BIM components defined by Γ_1 and Γ_2, and Daligault's fit [46] for the self-diffusion

$$D^*_{OCP} = \frac{a_0 + a_1\Gamma + a_2\Gamma^2 + a_3\Gamma^3}{b_0 + b_1\Gamma + b_2\Gamma^2 + b_3\Gamma^3}. \qquad (12b)$$

Coefficients can be found in [46]. Again, the corresponding kinetic self-diffusion of the effective BIM components are subtracted before applying the Darken mixing rule. A smooth transition across coupling regimes is then achieved at around $\Gamma_{\rm eff} = 0.15$.

C. Simple approach for EOS

For the PIJ, a simplified formulation of the equation of state of pure elements, as modeled by one component plasma (OCP), gives a reasonable estimation of the pressure in the multi-eV regime. The starting point is the estimation of the effective charge Q defined through the fit of the ionization given by More [47]. This fit could be improved to match more precisely OFMD results, but it leads to reasonably accurate results. The pressure is split into an ionic and electronic contributions. The ionic contribution is taken from the effective OCP and the electronic contribution is just the pressure of the electronic gas: $P_{\rm eff} = P_{\rm OCP} + P_{\rm e}$. The OCP pressure is given by the fit of Slattery *et al* [48] without the Madelung contribution

$$P_{\rm OCP}/nk_BT = 1 + \frac{1}{3}\left[b\Gamma^{1/4} + c\Gamma^{-1/4} + d\right], \qquad (13)$$

with b = 0.94544, c = 0.17954 and d = -0.80049. The Madelung term (-0.8975Γ) adds a contribution that gives a spurious negative ion pressure for coupling parameter greater than 4. This is a consequence of the rigid electronic background of the OCP model. For this reason, this term is not included in the ionic contribution. This leads to a good agreement with SESAME EOS in the hot dense regime.

For the electronic component, we use an interpolation formula between the Fermi gas and the perfect gas due to Nikiforov *et al* [49], with the effective ionization $n_e = Qn$,

$$P_{\rm ele}/n_e = \left[(k_BT)^3 + 3.36 n_e (k_BT)^{3/2} + \frac{9\pi^4}{125} n_e^2\right]^{1/3}, \qquad (14)$$

where atomic units are used for this latter (1 a.u. of pressure =294 Mbar). Knowing the density of pure hydrogen ρ_1 that gives the same pressure as pure silver at density ρ_2, the density for an arbitrary mixture is deduced as

$$\rho_{\rm mix} = \frac{x_1 A_1 + x_2 A_2}{x_1 V_1 + x_2 V_2}, \qquad (15)$$

where $V_1 = A_1/\rho_1$ and $V_2 = A_2/\rho_2$. Densities obtained with this model are in excellent agreement with Reference [5] isobar-isotherm model.

D. Scaling laws for pure species

In this section we represent transport coefficients as a function of temperature for pure species. Simulations

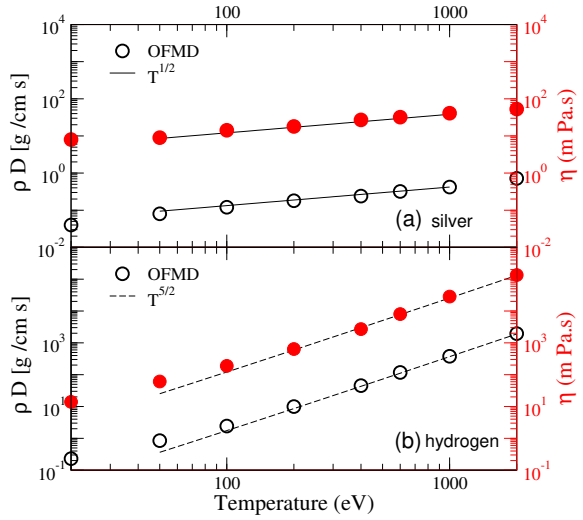

FIG. 2: (color online) Temperature scaling laws (17) for transport properties of silver (a) and hydrogen (b). Symbols are OFMD results (white open circles for diffusion and red filled circles for viscosity). Scaled diffusion, ρD is plotted on the left scale (black) and viscosity on the right scale (red).

on pure silver are done for the same density $20\,\mathrm{g/cm^3}$ between 20 and 2000 eV. We have shown in previous papers [50, 51] that below a critical value of 0.0045 of the reduced density ($\rho^* = \rho/AZ$, where Z and A are respectively the atomic number and the atomic weight), the coupling parameter Γ was constant in a wide range of temperature, at constant density. This regime, the Γ-plateau, corresponds to a balance between temperature and ionization, that scales as $T^{1/2}$ typically from 15 to 80% of full ionization (see Fig 1 (a), inset). The reduced coupling parameter $\Gamma^* = \Gamma/Z$, in the plateau, is a universal function of the reduced density and can be fitted by

$$\Gamma^* = b + a\ln[\rho^*], \tag{16}$$

where $a = 0.0695$ and $b = 0.714$. Silver at $20\,\mathrm{g/cm^3}$ corresponds to a reduced density of 0.00394 and hence must exhibit a plateau. Using the previous fit, we predict a coupling of about 15 between 100 and 600 eV. As shown in sec. II B, transport coefficients can be cast in an dimensionless form depending on Γ. The Γ-plateau thus corresponds to a constant value of diffusion and viscosity in plasmas units. To transform to real units ($\mathrm{cm^2/s}$ and Pa.s) one must multiply the diffusion by $\omega_p a^2$ and the viscosity by $nM\omega_p a^2$. For an isochoric transformation (as it is the case for silver) the only changing quantity is the plasma frequency proportional to the ionization Q, which scales as $T^{1/2}$, along the Γ-plateau. For silver, a scaling proportional to $T^{1/2}$ must be observed between 100 and 600 eV. The corresponding scaling law for silver appears in Fig. 2(a) for diffusion (where D_{Ag} is multiplied by a constant density of $20\,\mathrm{g/cm^3}$) and for viscosity .

Hydrogen, on the contrary, does not support a Γ-plateau and can be considered as fully ionized beyond a few tens of eV. Moreover, due to the isobaric constraint, the density of hydrogen varies between 0.88 and $3.81\,\mathrm{g/cm^3}$ with a coupling parameter always smaller than 0.1, above 100 eV. To eliminate the density dependency, we consider ρD. In the kinetic regime both diffusion and viscosity are given by the Fokker-Plank-Landau formula and scale as $T^{5/2}$ as shown in Fig. 2(b).

We find the following scaling laws

$$\begin{aligned} D_{Ag} &\propto T^{1/2} \quad \text{for} \quad 100 < T < 600\,\mathrm{eV} \\ \eta_{Ag} &\propto T^{1/2} \quad \text{for} \quad 100 < T < 600\,\mathrm{eV} \\ \rho D_H &\propto T^{5/2} \quad \text{for} \quad T > 200\,\mathrm{eV} \\ \eta_H &\propto T^{5/2} \quad \text{for} \quad T > 200\,\mathrm{eV}. \end{aligned} \tag{17}$$

These trends are reported in Fig. 2 (a) for silver and (b) for hydrogen and are in excellent agreement with OFMD data. They will be useful guidelines for analyzing mixtures properties.

III. RESULTS AND DISCUSSION FOR THE H-AG MIXTURE

A. EOS from OFMD simulations

Equation of state (EOS) is the relationship of pressure, temperature, volume, energy, and entropy. It is necessary to further understand the EOS of materials under extreme conditions because their properties will dramatically change. This study involves varying the concentration along an isobar-isotherm to map the change of the transport properties through a hypothetical interface. Usually mixtures simulations are performed by substitutions at constant volume leading to large changes in the pressure. This is particularly true for very asymmetric mixtures, where a small amount of the heavy element adds a large number of electrons, raising the pressure. The realization of isobaric mixtures requires changing the volume and hence the density of the mixture to realize a prescribed pressure. We present two approaches: the first one uses the simulation itself to find the density, and the second one uses a simplified, but analytical, equation of state as input to the PIJ model, see section II C.

Fig. 3 (a) shows the pressure as a function of concentration for each temperature. The black points are the OFMD pressure and the red dashed line is the target

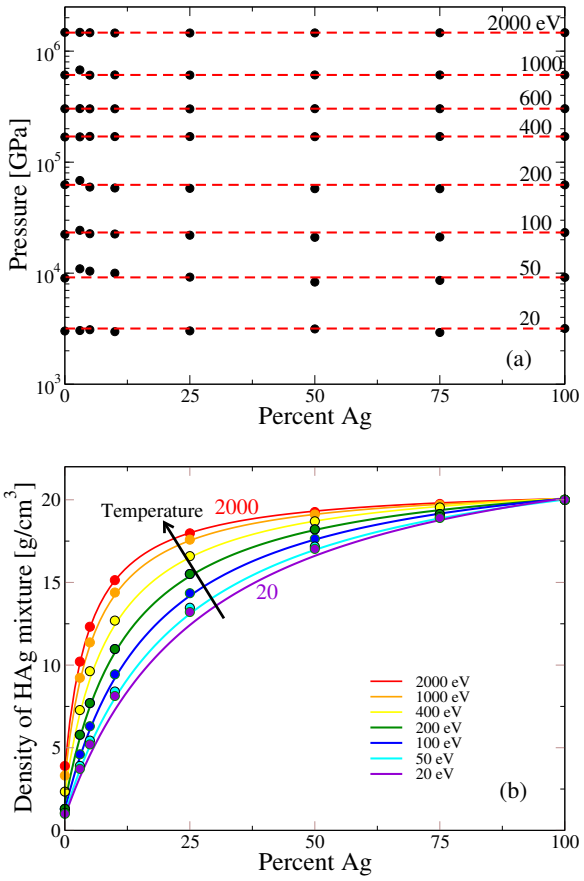

FIG. 3: (color online) (a) Pressure as a function of concentration for each temperature. The black points are the OFMD pressure and the red line is the target pressure. (b) Average atom TFD calculations, the density along a isobar as a function of concentration. Dots of corresponding colors are effective OCP evaluations of the mixture density.

pressure. The pressure matching was done to within 10%. The low concentration pressure matching was the most varied. At higher temperature, the pressure matching is better, near a few percent error. In general the transport properties are only weakly dependent on density, but highly dependent on concentration and temperature.

Fig. 3 (b) shows density from an average atom TFD calculation along isobars as a function of concentration. Starting at pure Ag, the density at low temperature (20 eV violet, lowest curve) gently bends over as it evolves to pure H. In contrast, at high temperature the system stays at higher densities even as H is added. Then the density quickly drops as the system approaches pure H (2000 eV red, highest curve).

Throughout the paper, when referring to an isobar, we mean the pressure matched simulations to pure Ag at 20 g/cm^3 for a given temperature.

B. Self and mutual diffusions versus concentration

We present the change in transport coefficients with evolving composition for the H-Ag mixtures. We first plot the transport properties versus concentration in percentage of the heavy element, for given temperatures. Then, we examine the behavior of these transport coefficients versus temperature, at a given concentration. To account for various densities and concentrations, we introduce specific combinations of variables to uncover general behaviors with respect to temperature.

We first examine the mutual and self-diffusions of the H-Ag system. In Fig. 4 we show the OFMD results as symbols for the self diffusion for Ag (red circles) and H (open circles), mutual diffusion (green diamonds), and the Darken estimate of mutual diffusion (blue circles) for varying concentrations along isobars at three temperatures: (a) 50, (b) 400, and (c) 1000 eV. PIJ predictions are shown by corresponding shaded areas and solid lines. For the sake of the demonstration, we have also reported in dashed lines, PIJ estimates without the H-Ag collision frequency for H self-diffusion.

For the pure H system, the H self-diffusion is largest. Then as Ag is added to the system, the H self-diffusion strongly decreases. For a pure Ag system, the Ag self-diffusion is 3 orders of magnitude smaller, and it weakly depends on the amount of H added. For the three temperatures considered here, the PIJ model predicts reasonably well the self diffusion of Ag. For hydrogen, we have plotted a shaded area corresponding to different choices of the relaxation coefficient R_1 (2 for the lower limit and 5 for the upper one). The lines within the shaded areas correspond to the estimate of R_1 from the limit of D_{12} when $x_2 \to 1$. Despite this dispersion, the PIJ model predicts very well the huge reduction of the H self diffusion produced by the introduction of a very small amount of Ag. We note that the 50 eV case ($\Gamma_H \simeq 0.3$) is less sensitive to variations in the kinetic contribution of the PIJ model. At 400 eV there is a transition from the correlated regime to the kinetic one. In this transitory regime, the PIJ model is sensitive to the choice of the bounding of the Coulomb logarithm Ł_0. Changing this threshold from to 2 to 3 would degrade the agreement with data at 400 eV. At higher temperature, 1000 eV, the agreement is very good since hydrogen is in the fully kinetic regime and silver still correlated.

Looking at the mutual diffusion in Fig. 4 (green symbols). When the system is nearly pure H, the mutual diffusion should approach the Ag self diffusion as a lower limit, but depending on the temperature, the mutual diffusion can still much larger. For small amounts of Ag, the mutual diffusion approaches the Ag self-diffusion as the fraction of Ag vanishes. We more clearly see this behavior in the PIJ model (solid lines). As Ag is added, the mutual diffusion increases until the mutual diffusion is at its largest value nearly equally to the H self-diffusion. This behavior is in line with the Darken relation, Eq. (4), and these results are shown in blue symbols for Fig. 4.

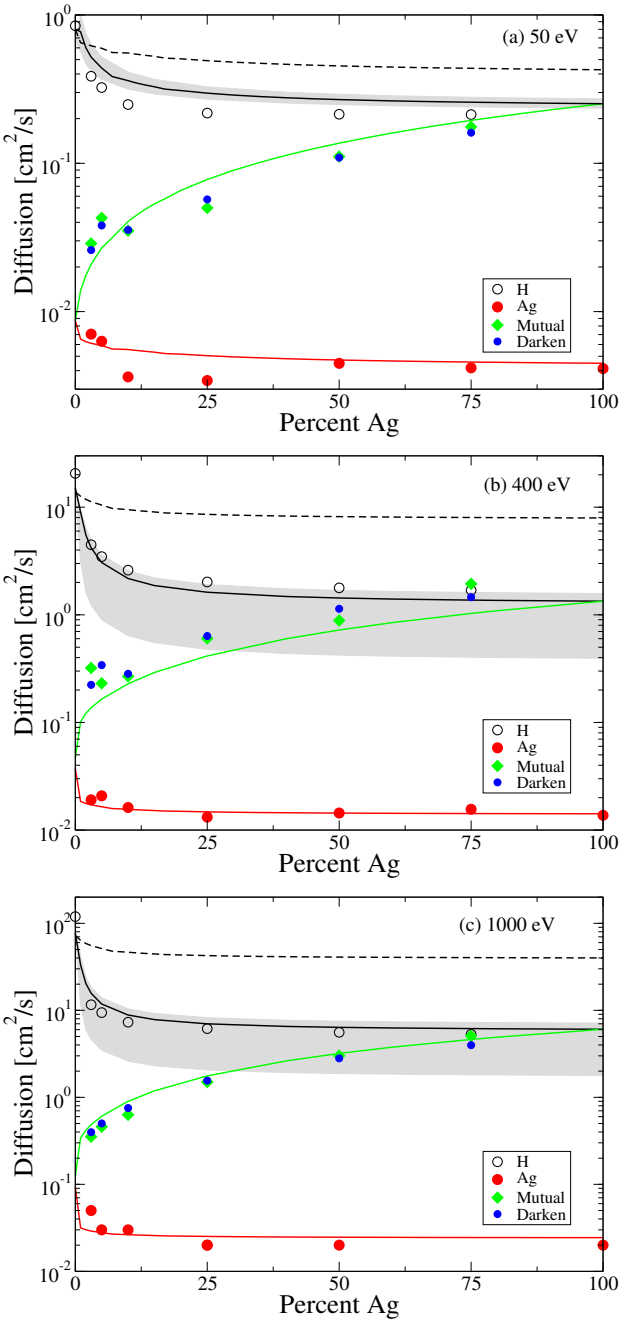

FIG. 4: (color online) The OFMD diffusion as a function of percent Ag for H (open circles) and Ag (red circles), mutual diffusion (green diamonds),and Darken estimate of mutual diffusion (blue circles) along isobars are shown for three temperatures: (a) 50, (b) 400, and (c) 1000 eV. The PIJ predictions are shown by corresponding solid lines. The shaded area correspond to the uncertainty for relaxation correction: 2 lower limit and 5 upper limit. Additionally, we show the H self-diffusion without the H-Ag collision frequency as a dashed curve.

Note the Darken relation uses the self-diffusions from the full mixture, not the self-diffusions from the pure species

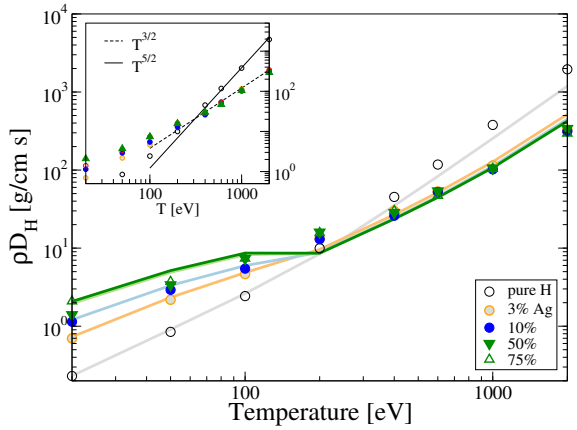

FIG. 5: (color online) ρ D_H from OFMD versus temperature for hydrogen mixed with increasing percentage of Ag compared with PIJ model (lines with corresponding colors). Inset: power law scaling with temperature.

simulations. The Darken relation respects the limiting behavior of D_{12} at extreme dilution. For this reason, it is a good interpolation formula.

Also shown in Fig. 4 is hydrogen self-diffusion without the cross terms H-Ag in the collision frequency (dashed lines). These curves show that the common method of estimating the transport properties can be inaccurate, dramatically over predicting the self-diffusion. This is important when considering the Darken relationship, Eq. 4. This result highlights the importance of using the self-diffusion coefficients from simulations of the full mixture, this is particularly acute for the light element. It further highlights the importance of including the modified H-Ag collision frequency for hydrogen's self-diffusion in the PIJ model.

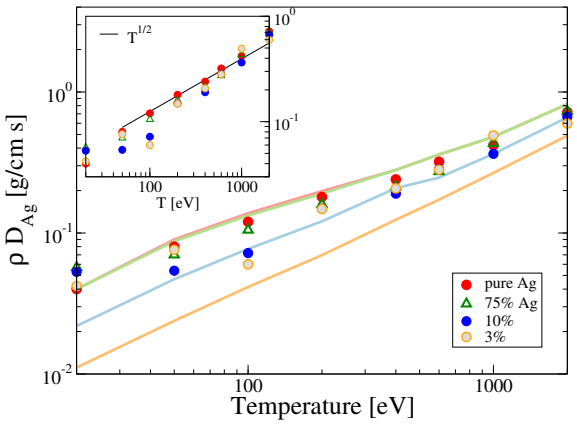

FIG. 6: (color online) ρD_{Ag} from OFMD (symbols) versus temperature for silver mixed with increasing percentage of H compared with PIJ model (lines with corresponding colors). Inset: the $T^{1/2}$ law is the consequence of the ionization of silver in the Γ plateau.

C. Self-diffusion versus temperature

Trends of diffusion versus temperature are well identified if we plot ρD versus T as shown in Figs. 5 and 6. In Fig. 5 we show the temperature dependence of H self-diffusion times the density for various silver concentrations: 0 (open circles), 3 (open orange circles), 10 (blue circles), 50 (green down triangles) and 75 (green up triangles) % Ag by number.

For hydrogen the situation is explicit. Pure hydrogen follows kinetic scaling as soon as the temperature goes beyond 200 eV. However if a small amount of silver is introduced, the power law switches to $T^{3/2}$, which holds for all considered concentrations with a very low dispersion beyond 200 eV. This is the signature of a qualitative change from the diffusion of a pure OCP plasma to a Lorentz type diffusion of hydrogen between heavy, strongly charged silver atoms. This behavior is traced back to the dominant collision frequency ν_{12}, which scales as $Q^2T^{-3/2}$, giving a diffusion coefficient, Eqn. (9c), scaling as $T^{3/2}/Q^2 \times T$ and hence as $T^{3/2}$ since on the Γ plateau the ionization scales as $Q \propto T^{1/2}$. We emphasize that kinetic formula can be used here since H is characterized by a coupling parameter less than 0.1 as soon as the temperature is greater than 100 eV, see Fig. 1 (b). In short, the change from 5/2 to 3/2 is simply due to the appearance of a new dominant contribution (scaling as Q^2) to the collision frequency. The PIJ model reproduces these trends and gives the transition between the kinetic regime (hydrogen beyond 400 eV) and the correlated regime (mixture below 200 eV). For pure hydrogen, the agreement with data at high temperature is not perfect and could be improved by another choice of the relaxation correction and coupling threshold (L_0=3.5 and R_H=1.7 yields a perfect agreement for pure hydrogen at all temperatures at the expense of mixture properties). This raises the question of the best choice of the Coulomb logarithm thresholds in mixtures.

In Fig. 6 we show the temperature dependence of Ag self-diffusion multiplied by the density for various concentrations: 100 (red dots), 3 (orange circles), 10 (blue circles), and 75 (green up triangle) % silver by number. in contrast with hydrogen, silver always stays in the correlated regime. We have seen in Fig. 2 (a) that between 100 to 600 eV the diffusion of pure silver scales as $T^{1/2}$, reflecting the increase of the ionization along the Γ-plateau. The addition of a light element to the mixture has a weak effect, and ρD_{Ag} remains close to a $T^{1/2}$ scaling. At very low concentration of silver and lower temperature, we note a larger discrepancy, up to a factor of 3, between silver self-diffusion and PIJ predictions.

D. Mutual diffusion versus temperature

We conclude from the Sec. III B that, first, the Darken relation provides a good estimation of the mutual diffusion and, second, that the self diffusion of the heavy component is about two orders of magnitude smaller that the light one. Thus, we can write for asymmetric mixtures $D_{12} \simeq xD_1$ and deduce the correct density scaled mutual diffusion $\rho D_{12}/x$. The consequence is that the mutual diffusion is essentially kinetic in contrast with the viscosity which is driven by correlation. Using this scaling we observe that all points gather on the same line in Fig. 7, whatever the concentration x in heavy element: 5% (orange circles), 25 % (blue diamonds) and 75% (green triangles). The density scaled mutual diffusion only depends on the temperature and can be estimated through kinetic formulation of the PIJ model. Beyond 200 eV, if we suppose that Ag ionization Q scales as $T^{1/2}$, we get a scaling of D_{12} as $T^{3/2}$, compatible with data in Fig. 7. PIJ model predictions are also merging beyond 200 eV (kinetic regime) and close to the data but a larger dispersion is observed at low temperature.

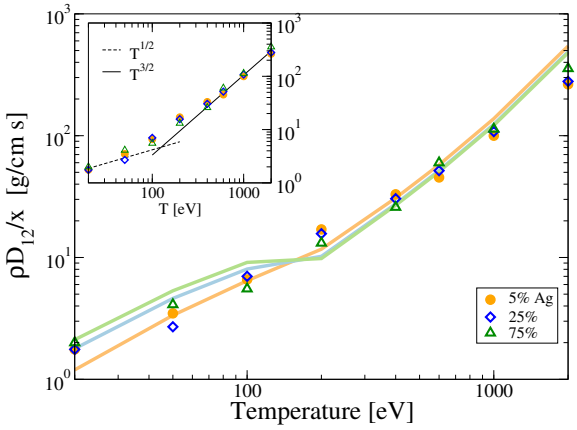

FIG. 7: (color online) Temperature dependence of the OFMD $\rho D_{12}/x$ for various levels of concentration x : 5% (orange circles), 25 % (blue diamonds) and green up triangles (75%). Inset: power laws $T^{3/2}$ for the solid line and $T^{1/2}$ for the dashed line.

E. Viscosity versus concentration

Fig. 8 shows the behavior of the viscosity along isobars, see section III A, as a function of Ag concentration for three temperatures: 50 eV (black open circles), 400 eV (blue open squares), and 1000 (red open triangles) eV. At low temperatures the ratio between the viscosity for pure hydrogen and pure silver is small, at 20 eV (not shown) it is just over a factor of 2 and for 50 eV it is just under a factor of 7. But at 1000 eV, the change in viscosity is about a factor of 700 and for 2000 eV (not shown), it is a factor of 2500. This behavior is reproduced well by the PIJ model (solid lines).

It is also interesting to see how much the viscosity changes with just a small amount of added silver. For example at 1000 eV, the viscosity drops an order of magnitude with the addition of 3% Ag. The comparison with

Fig. 1 (b) immediately suggests that this effect is just a matter of collision frequencies, Ag ions being the dominant scatterers. This effect, already observed for asymmetric BIMs [14], is not nearly as pronounced at low temperature. At 20 eV the difference in viscosity from simulations with 100 % H and 97% H is 23% and at 50 eV it is just under a factor of 2. When the system contains more silver than hydrogen, any further change to the viscosity is gradual.

F. Viscosity versus temperature

Fig. 9 (a) shows the temperature dependence of viscosity for various concentrations. For pure hydrogen at high temperature the viscosity scales as $T^{5/2}$ as discussed in the previous section. We recognize the $T^{1/2}$ behavior for pure Ag, as predicted by the Γ-plateau model. The difference between these two limits is striking. These two behaviors are captured by the PIJ model because the kinetic limit and the Γ-plateau are included. PIJ predictions are less accurate for low concentration mixtures that are also much more difficult to simulate due to statistics.

When $x\eta/\rho$ is plotted versus temperature, the viscosity points, that were scattered in Fig. 9 (a), are now grouped along two main lines in Fig. 9 (b), characteristic of two well-identified behaviors. While pure hydrogen always stays in the kinetic regime with a power law $T^{5/2}$, a small amount of silver changes the scaling to a dependence not far from $T^{1/2}$, which is the signature of the Γ-plateau. Even at very low silver concentration (3%) the behavior of the viscosity is the one of a strongly correlated plasma.

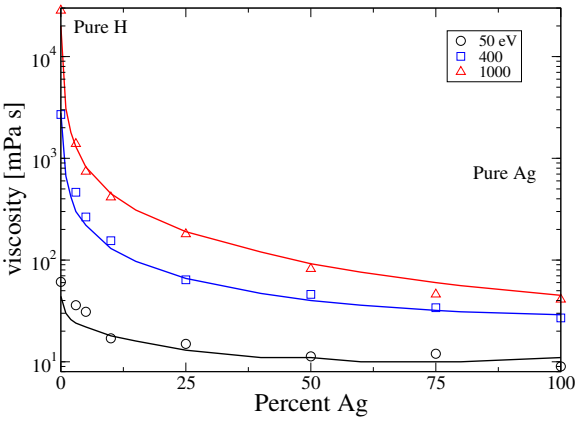

FIG. 8: (color online) The viscosity from OFMD simulations along isobars, see section III A, as a function of percent Ag for three temperatures 50 (black squares), 400 (blue squares), and 1000 eV (red squares) . Lines of corresponding colors are PIJ evaluations.

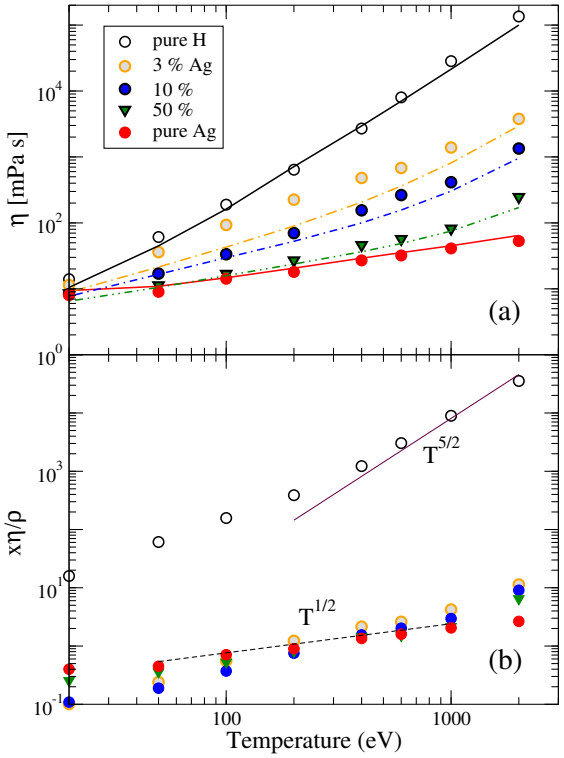

FIG. 9: (color online) (a) Viscosity as a function of temperature for both the PIJ model (lines) and OFMD simulations (symbols) at different concentrations: pure H (open circles), 3 (orange circles), 10 (blue circles), 50% (green down triangles), and pure Ag (red circles). (b) $x\,\eta/\rho$ versus T. Lines represent the $T^{5/2}$ and $T^{1/2}$ scalings.

IV. CONCLUSION

We have presented a series of simulations of hydrogen-silver mixtures in the orbital-free molecular dynamics framework. For each temperature, ranging from 20 to 2000 eV, the densities have been obtained through an isobaric constraint to target the pure silver pressure, see section III A. We have obtained diffusion coefficients and viscosities and have shown the tremendous effect of a small amount of heavy element. Simulations are compared with the theoretical PIJ model which succeeds in explaining these strong variations. Additionally, the sudden change in the temperature scaling law, when a heavy element is added is clarified within the PIJ modeling as a direct consequence of the cross H-Ag contribution to the collision frequencies. The particular case of strong asymmetric mixtures bring simplifications. When $D_H \gg D_{Ag}$, the Darken relation reduces to a mutual diffusion coefficient given by xD_H, where x is the Ag concentration. Interestingly, the mutual diffusion is essentially kinetic and the viscosity is correlated.

Future work will be to improve the microscopic description of the mixture through a detailed study of the system. This will include looking at the pair distribu-

tion function and the velocity auto correlation functions for such mixtures as concentration changes. It will hold valuable insights into the behavior of such mixtures and how they relate to basic model systems [52].

Acknowledgments

The authors gratefully acknowledge support from Advanced Simulation and Computing, Science Campaign 4, computing resource from CCC, and LANL which is operated by LANS, LLC for the NNSA of the U.S. DOE under Contract No. DE-AC52-06NA25396. This work has been performed under the NNSA/DAM collaborative agreement P184 on Basic Science. We especially thank Flavien Lambert for providing his OFMD code.

Appendix: Parametrization of relaxation corrections

In the weakly coupled regime, the kinetic equations can be used to compute transport coefficients. The procedure consists in linearizing the kinetic equations around equilibrium and solving for the response to small gradients in temperature velocity and concentrations. Following Decoster [43] we get for the viscosity

$$\eta_{12}^{(1)} = K_1 \frac{n_1\ k_B T_1}{\nu_{11}+\nu_{12}} + K_2\ \frac{n_2\ k_B T_2}{\nu_{22}+\nu_{21}}. \qquad \text{(A.1)}$$

$K_1 = \xi(y)$ and $K_2 = 0.965$

$$y = \frac{\nu_{12}}{\sqrt{2}\ \nu_{11}}\ \simeq\ \frac{n_2\ Q_2^2}{n_1\ Q_1^2}\ =\ \frac{x\ Q^2}{1-x}. \qquad \text{(A.2)}$$

Q_1 and Q_2 are the ionizations and $x = N_2/N$. The coefficient $\xi(y)$ is given by the following relation [43, 53]

$$\xi(y) = \frac{5}{6}\ \frac{(204\sqrt{2}\ y + 205)(y + 1/\sqrt{2})}{96\sqrt{2}\ y^2 + 301\ y + 89\sqrt{2}}, \qquad \text{(A.3)}$$

and varies between 1 and 2. For the mutual diffusion

$$D_{12}^{\mathrm{FPL}} = R_{12}\ c_2\ \frac{k_B T}{\nu_{12}}\ \frac{\overline{m}}{m_1 m_2}, \qquad \text{(A.4)}$$

the coefficient $R_{12}(y)$ is given by $R_{12} = 1/\chi(y)$ with the following fit [43]

$$\chi(y) = \frac{(3\pi/32)\ y^2 + 0.8783\ y + 0.304}{y^2 + 1.609\ y + 0.304}, \qquad \text{(A.5)}$$

and varies between 1 and 3.5.
In the lack of theoretical estimation for R_1, we assumed that it does not depend on the concentration and used the limit of the mutual diffusion coefficient at infinite hydrogen dilution $\lim_{x\to 1} D_{12} = D_1$, which gives $R_1 \simeq 3.5$. Of course, this is a crude approximation since for pure elements R_1=1.19. These fits are implemented in PIJ model.

[1] V. A. Smalyuk, L. J. Atherton, L. R. Benedetti, R. Bionta, D. Bleuel, E. Bond, D. K. Bradley, J. Caggiano, D. A. Callahan, D. T. Casey, et al., Phys. Rev. Lett. **111**, 215001 (2013), URL http://link.aps.org/doi/10.1103/PhysRevLett.111.215001.

[2] M. J. Edwards, P. K. Patel, J. D. Lindl, L. J. Atherton, S. H. Glenzer, S. W. Haan, J. D. Kilkenny, O. L. Landen, E. I. Moses, A. Nikroo, et al., Physics of Plasmas (1994-present) **20**, 070501 (2013), URL http://scitation.aip.org/content/aip/journal/pop/20/7/10.1063/1.4816115.

[3] H. F. Robey, B. J. MacGowan, O. L. Landen, K. N. LaFortune, C. Widmayer, P. M. Celliers, J. D. Moody, J. S. Ross, J. Ralph, S. LePape, et al., Physics of Plasmas (1994-present) **20**, 052707 (2013), URL http://scitation.aip.org/content/aip/journal/pop/20/5/10.1063/1.4807331.

[4] H. G. Rinderknecht, H. Sio, C. K. Li, A. B. Zylstra, M. J. Rosenberg, P. Amendt, J. Delettrez, C. Bellei, J. A. Frenje, M. Gatu Johnson, et al., Phys. Rev. Lett. **112**, 135001 (2014), URL http://link.aps.org/doi/10.1103/PhysRevLett.112.135001.

[5] K. Molvig, E. L. Vold, E. S. Dodd, and S. C. Wilks, Phys. Rev. Lett. **113**, 145001 (2014), URL http://link.aps.org/doi/10.1103/PhysRevLett.113.145001.

[6] K. Molvig, A. N. Simakov, and E. L. Vold, Physics of Plasmas **21**, 092709 (2014), URL http://scitation.aip.org/content/aip/journal/pop/21/9/10.1063/1.4895666.

[7] L. Welser-Sherrill, J. Fincke, F. Doss, E. Loomis, K. Flippo, D. Offermann, P. Keiter, B. Haines, and F. Grinstein, High Energy Density Physics **9**, 496 (2013), ISSN 1574-1818, URL http://www.sciencedirect.com/science/article/pii/S157418181300061X.

[8] D. Bruno, C. Catalfamo, M. Capitelli, G. Colonna, O. De Pascale, P. Diomede, C. Gorse, A. Laricchiuta, S. Longo, D. Giordano, et al., Physics of Plasmas **17**, 112315 (2010), URL http://scitation.aip.org/content/aip/journal/pop/17/11/10.1063/1.3495980.

[9] J. Hughto, A. S. Schneider, C. J. Horowitz, and D. K. Berry, Phys. Rev. E **82**, 066401 (2010), URL http://link.aps.org/doi/10.1103/PhysRevE.82.066401.

[10] F. Lambert, J. Clérouin, J.-F. Danel, L. Kazandjian, and G. Zérah, Phys. Rev. E **77**, 026402 (2008), URL http://link.aps.org/doi/10.1103/PhysRevE.77.026402.

[11] L. Burakovsky, C. Ticknor, J. D. Kress, L. A. Collins, and F. Lambert, Phys. Rev. E **87**, 023104 (2013), URL http://link.aps.org/doi/10.1103/PhysRevE.87.023104.

[12] J.-F. Danel and L. Kazandjian, Phys. Rev. E **91**, 013103 (2015), URL http://link.aps.org/doi/10.

	pure hydrogen		3% Ag			10% Ag			50% Ag			75% Ag			pure silver	
T	ρ	ρD_H	ρ	ρD_H	ρD_{Ag}	ρ	ρD_H	ρD_{Ag}	ρ	ρD_H	ρD_{Ag}	ρ	ρD_H	ρD_{Ag}	ρ	ρD_{Ag}
20	0.88	0.23	3.40	0.70	0.042	7.60	1.14	0.053	16.90	1.40	0.053	19.00	2.09	0.057	20.	0.040
50	1.00	0.85	4.50	2.18	0.076	9.00	2.92	0.054	15.80	3.38	0.063	17.50	3.72	0.070	20.	0.080
100	1.20	2.43	5.00	4.65	0.060	9.00	5.46	0.072	16.00	7.33	0.096	17.60	7.39	0.105	20.	0.120
200	1.65	9.97	5.50	13.2	0.148	9.30	13.00	0.149	16.70	16.00	0.167	17.80	15.70	0.160	20.	0.180
400	2.20	45.30	6.70	29.90	0.207	10.00	26.00	0.190	16.00	28.50	0.208	17.80	30.10	0.213	20.	0.240
600	2.63	117.70	7.83	53.10	0.281	13.05	52.42	0.284	18.80	53.90	0.301	19.56	47.00	0.273	20.	0.320
1000	3.17	378.60	9.85	114.20	0.492	14.00	102.00	0.364	19.00	106.00	0.400	19.66	104.20	0.432	20.	0.420
2000	3.81	1952.60	9.97	327.00	0.598	14.80	313.00	0.666	19.10	340.00	0.706	19.68	295.00	0.728	20.	0.720

TABLE I: Self-diffusion of hydrogen and silver multiplied by the density of the mixture given by the isobaric prescription, see section III A. T in eV, ρD_H and ρD_{Ag} in g/cm s as obtained in OFMD simulations.

1103/PhysRevE.91.013103.

[13] F. Lambert and V. Recoules, Phys. Rev. E **86**, 026405 (2012), URL http://link.aps.org/doi/10.1103/PhysRevE.86.026405.

[14] J. G. Clérouin, M. H. Cherfi, and G. Zérah, Europhys. Lett. **42**, 37 (1998).

[15] S. Bastea, Phys. Rev. E **71**, 056405 (2005), URL http://link.aps.org/doi/10.1103/PhysRevE.71.056405.

[16] S. Bastea, Phys. Rev. E **75**, 031201 (2007), URL http://link.aps.org/doi/10.1103/PhysRevE.75.031201.

[17] P. Arnault, High Energy Density Physics **9**, 711 (2013), URL http://www.sciencedirect.com/science/article/pii/S1574181813001651.

[18] L. G. Stanton and M. S. Murillo, Phys. Rev. E **93**, 043203 (2016), URL http://link.aps.org/doi/10.1103/PhysRevE.93.043203.

[19] T. Haxhimali, R. E. Rudd, W. H. Cabot, and F. R. Graziani, Phys. Rev. E **90**, 023104 (2014), URL http://link.aps.org/doi/10.1103/PhysRevE.90.023104.

[20] T. Haxhimali, R. E. Rudd, W. H. Cabot, and F. R. Graziani, Phys. Rev. E **92**, 053110 (2015), URL http://link.aps.org/doi/10.1103/PhysRevE.92.053110.

[21] C. E. Starrett and D. Saumon, Phys. Rev. E **85**, 026403 (2012), URL http://link.aps.org/doi/10.1103/PhysRevE.85.026403.

[22] C. E. Starrett, D. Saumon, J. Daligault, and S. Hamel, Phys. Rev. E **90**, 033110 (2014), URL http://link.aps.org/doi/10.1103/PhysRevE.90.033110.

[23] C. E. Starrett, J. Daligault, and D. Saumon, Phys. Rev. E **91**, 013104 (2015), URL http://link.aps.org/doi/10.1103/PhysRevE.91.013104.

[24] A. Pribram-Jones, S. Pittalis, E. Gross, and K. Burke, in *Frontiers and Challenges in Warm Dense Matter*, edited by F. Graziani, M. P. Desjarlais, R. Redmer, and S. B. Trickey (Springer International Publishing, 2014), vol. 96 of *Lecture Notes in Computational Science and Engineering*, pp. 25–60, ISBN 978-3-319-04911-3, URL http://dx.doi.org/10.1007/978-3-319-04912-0_2.

[25] S. A. Bonev, B. Militzer, and G. Galli, Phys. Rev. B **69**, 014101 (2004), URL http://link.aps.org/doi/10.1103/PhysRevB.69.014101.

[26] B. Militzer and K. P. Driver, Phys. Rev. Lett. **115**, 176403 (2015), URL http://link.aps.org/doi/10.1103/PhysRevLett.115.176403.

[27] F. Lambert, J. Clérouin, and G. Zérah, Phys. Rev. E **73**, 016403 (2006), URL http://link.aps.org/doi/10.1103/PhysRevE.73.016403.

[28] J. D. Kress, J. S. Cohen, D. A. Horner, F. Lambert, and L. A. Collins, Phys. Rev. E **82**, 036404 (2010), URL http://link.aps.org/doi/10.1103/PhysRevE.82.036404.

[29] J. D. Kress, J. S. Cohen, D. P. Kilcrease, D. A. Horner, and L. A. Collins, Phys. Rev. E **83**, 026404 (2011), URL http://link.aps.org/doi/10.1103/PhysRevE.83.026404.

[30] D. A. Horner, J. D. Kress, and L. A. Collins, Phys. Rev. B **77**, 064102 (2008), URL http://link.aps.org/doi/10.1103/PhysRevB.77.064102.

[31] D. A. Horner, F. Lambert, J. D. Kress, and L. A. Collins, Phys. Rev. B **80**, 024305 (2009), URL http://link.aps.org/doi/10.1103/PhysRevB.80.024305.

[32] C. Ticknor, L. A. Collins, and J. D. Kress, Phys. Rev. E **92**, 023101 (2015), URL http://link.aps.org/doi/10.1103/PhysRevE.92.023101.

[33] C. Ticknor, S. D. Herring, F. Lambert, L. A. Collins, and J. D. Kress, Phys. Rev. E **89**, 013108 (2014), URL http://link.aps.org/doi/10.1103/PhysRevE.89.013108.

[34] C. Wang, Z. Li, D. Li, and P. Zhang, Physics of Plasmas **22**, 102702 (2015), URL http://scitation.aip.org/content/aip/journal/pop/22/10/10.1063/1.4931994.

[35] P. Minary, G. J. Martyna, and M. E. Tuckerman, The Journal of Chemical Physics **118**, 2510 (2003), URL http://scitation.aip.org/content/aip/journal/jcp/118/6/10.1063/1.1534582.

[36] F. Perrot, Phys. Rev. A **20**, 586 (1979), URL http://link.aps.org/doi/10.1103/PhysRevA.20.586.

[37] J. P. Perdew and A. Zunger, Phys. Rev. B **23**, 5048 (1981), URL http://link.aps.org/doi/10.1103/PhysRevB.23.5048.

[38] M. P. Allen and D. J. Tildesley, *Computer Simulations of Liquids* (Oxford University Press, 2009).

[39] D. Alfè and M. J. Gillan, Phys. Rev. Lett. **81**, 5161 (1998), URL http://link.aps.org/doi/10.1103/PhysRevLett.81.5161.

[40] E. R. Meyer, J. D. Kress, L. A. Collins, and C. Ticknor, Phys. Rev. E **90**, 043101 (2014), URL http://link.aps.org/doi/10.1103/PhysRevE.90.043101.

[41] R. Zwanzig and N. K. Ailawadi, Phys. Rev. **182**, 280 (1969), URL http://link.aps.org/doi/10.1103/PhysRev.182.280.

[42] E. M. Lifshitz and L. P. Pitaevskii, *Physical Kinetics* (Pergamon Press, Oxford, 1981).

[43] A. Decoster, P. A. Markowich, B. Perthame, and P.-A. Raviart, *Modeling of collisions*, Series in applied mathematics (Gauthier-Villars, Paris, 1998), ISBN 2-8429-9067-6, copyright 1998 : Editions scientifiques et médicales Elsevier, URL http://opac.inria.fr/record=b1094490.

[44] S. I. Braginskii, Reviews of Plasma Physics **1**, 205 (1965).

[45] R. M. More, Preprint UCRL UCRL-84991, Lawrence Livermore Laboratory, Lawrence Livermore National Laboratory (1981).

[46] J. Daligault, Phys. Rev. Lett. **96**, 065003 (2006), URL http://link.aps.org/doi/10.1103/PhysRevLett.96.065003.

[47] D. Salzmann, *Atomic Physics in Hot Plasmas* (Oxford University Press, Oxford, 1998).

[48] W. L. Slattery, G. D. Doolen, and H. E. DeWitt, Phys. Rev. A **21**, 2087 (1980), URL http://link.aps.org/doi/10.1103/PhysRevA.21.2087.

[49] A. F. Nikiforov, V. G. Novikov, and V. B. Urarov, *Quantum-Statistical Models of Hot Dense Matter* (Birkhauser, Basel, 2005).

[50] P. Arnault, J. Clérouin, G. Robert, C. Ticknor, J. D. Kress, and L. A. Collins, Phys. Rev. E **88**, 063106 (2013), URL http://link.aps.org/doi/10.1103/PhysRevE.88.063106.

[51] J. Clérouin, G. Robert, P. Arnault, J. D. Kress, and L. A. Collins, Phys. Rev. E **87**, 061101 (2013), URL http://link.aps.org/doi/10.1103/PhysRevE.87.061101.

[52] J. Clérouin, P. Arnault, C. Ticknor, J. D. Kress, and L. A. Collins, Phys. Rev. Lett. **116**, 115003 (2016), URL http://link.aps.org/doi/10.1103/PhysRevLett.116.115003.

[53] R. R.Balescu, *Transport Processes in Plasmas. 1.Classical Transport Theory* (North Holland, Amsterdam, 1988).